

Negative mobility, sliding, and delocalization for stochastic networksDima Boriskovsky and Doron Cohen *Department of Physics, Ben-Gurion University of the Negev, Beer-Sheva 84105, Israel*

(Received 15 December 2019; revised manuscript received 31 March 2020; accepted 2 June 2020; published 17 June 2020)

We consider prototype configurations for quasi-one-dimensional stochastic networks that exhibit negative mobility, meaning that current decreases or even reversed as the bias is increased. We then explore the implications of disorder. In particular, we ask whether lower and upper bias thresholds restrict the possibility to witness nonzero current (sliding and antisliding transitions, respectively), and whether a delocalization effect manifests itself (crossover from over-damped to under-damped relaxation). In the latter context detailed analysis of the relaxation spectrum as a function of the bias is provided for both on-chain and off-chain disorder.

DOI: [10.1103/PhysRevE.101.062129](https://doi.org/10.1103/PhysRevE.101.062129)**I. INTRODUCTION**

Negative mobility, where a system respond to the bias in an opposite way to the naive expectation, has been studied experimentally long ago for semiconductors, diodes, and superlattices that feature resonance tunneling [1–4] or carriers with negative effective mass [5–8]. But it has been realized that such effect can be expected also for a purely stochastic hopping conductance in the presence of high electric field [9]. The physics involved is that of biased diffusion in random structures such as percolating systems above criticality. The essential physics is captured by simpler quasi-one-dimensional configurations, notably by *comb or tree structures* that feature random distribution of dangling branches or waiting times [10–13] (and see further references therein). Negative mobility can be described as “getting less from pushing more,” and there is a possibility of observing an upper critical bias beyond which the drift velocity vanishes. More complicated configurations have been considered as well, for example: the flow of particles through a narrow tube with hooks that provide trapping mechanism [14]; inertial tracers in steady laminar flows [15]; kinetically constrained systems [16,17]; possibly involving several species of carriers [18] or mixture of gases [19]. Most of the cited examples above refer to negative differential mobility (NDM), but some also to absolute negative mobility (ANM), notably Brownian motors [20–22]. The latter are required to be nonequilibrium, or active systems in some sense [23,24]. We further illuminate the latter observation below.

A. Objective

In the present work we consider *minimal* stochastic models where either NDM or ANM can be expected. Those are illustrated in Fig. 1. In both cases the configuration reflects the existence of more than one dimension, as opposed to a simple one-dimensional chain with near-neighbor transitions. The NDM configuration of Fig. 1(b) is a minimal comb structure of the type that has been studied in the past [10–13,23]. The ANM configuration of Fig. 1(c) is

a simplified version of Ref. [23] that has been studied in Ref. [24]. The ANM configuration is further characterized by a nontrivial topology. Namely, it is an active stochastic network that features loops, around which the circulation of the stochastic field is nonzero. It can represent the dynamics of a Janus particle [25–27] in one dimension [24,28], where the extra degree of freedom is its orientation. Our main interest concerns the implication of disorder on the stochastic relaxation. We provide below some background to the relevant literature, followed by an outline that explains our motivation to further study the prototype configuration of Fig. 1(b), which complements our previous studies [24,29] of relaxation for the configurations Figs. 1(a) and 1(c), respectively.

B. Sinai model

The study of stochastic motion on a one-dimensional random lattice with near-neighbor transitions has been introduced by Sinai [30], a.k.a., *random walk in random environment*. The model is illustrated in Fig. 1(a). Unlike Einstein’s Brownian motion, here the rates of transition between two adjacent sites do not have to be the same in both directions. This can be regarded as arising from a *stochastic field*, due to a potential difference that biases the transitions. If the stochastic field is uncorrelated on different bonds, then it follows that the potential is characterized by an activation barrier whose height scales as \sqrt{L} , where L is the length of the sample. It follows that the steady-state current is $I \sim \exp[-\text{const}\sqrt{L}]$, and not $I \propto 1/L$. In time domains it implies subdiffusion $R \sim \ln^2(t)$, where R is the distance that is covered by the particle during time t . This differs completely from the usual random walk result $R \sim t^{1/2}$.

C. Sliding transition

Adding bias in the context of Sinai model means that the rates in one direction (say to the right) are, on the average, larger than the rates of transition in the opposite direction. It turns out that the system exhibits a nonzero drift velocity v provided the bias exceeds a finite critical value. This is

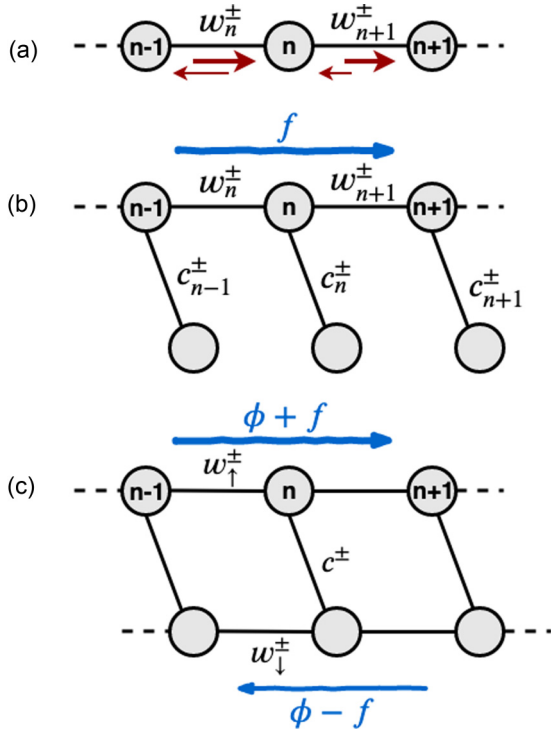


FIG. 1. Schematic drawing of the model system. (a) The standard Sinai model, namely, one-dimensional chain where the transition-rates have independent random values. (b) One-dimensional chain with dangling bonds that serves as a minimal model for a stochastic percolating network. (c) Quasi-one-dimensional network that serves as a minimal model for an active gas of Janus-type particles. In panel (a) the rates are indicated by arrows. Such arrows are omitted in panels (b, c) where we prefer to indicate the preferred direction of transitions due to the external bias and the self-propulsion. In the absence of disorder the model parameters in panel (a) are the transition rate w_o for unbiased transitions, and the bias field f that encourages motion to the right. Sinai disorder means that f acquires an uncorrelated random component. In panel (b) we have additional dangling bonds. If those transition rates are random, then we call it “off chain disorder.” In panel (c) we also have propulsion ϕ that encourages the motion to be in a direction that agrees with the orientation of the particle. See text for further details, and Eqs. (2)–(9) for precise definition of the model parameters.

known as the *sliding transition* [31]. For subcritical bias the drift is $R \sim t^\mu$, where $\mu \in [0, 1]$ depends on the bias. For a comprehensive review, see Refs. [32,33]. Here we focus on the possibility that above some second critical bias the drift velocity becomes zero again, relating to the minimal configuration of Fig. 1(b).

D. Delocalization transition

Somewhat related to the sliding transition is the delocalization transition of the relaxation modes. Here one considers a ring geometry: a chain segment with periodic boundary conditions. The delocalization transition has been discussed originally for non-Hermitian Hamiltonians [34–36] and only later for stochastic chains [37]. In the next paragraph we explain the term delocalization in the latter context.

In the presence of bias (a.k.a., affinity), due to the disorder, some (or all) eigenvalues become real, which is regarded as an indication for the localization of the associated eigenmodes. As the bias is increased, some of those real eigenvalues become complex, which is termed delocalization transition. The delocalization of the eigenmodes whose eigenvalues reside in the vicinity of $\lambda = 0$ implies that the relaxation become under-damped (with oscillations). As explained in Ref. [37], the threshold for that is lower than the threshold for the sliding transition (it corresponds to $\mu = 1/2$ and not to $\mu = 1$).

The delocalization of the relaxation modes for the active network of Fig. 1(c) has been already studied in Ref. [24]. Here we focus on the configuration of Fig. 1(b), and distinguish between on-chain disorder and off-chain disorder. This part of the study is motivated by the following question: We know that in one dimension we always have localization; does it mean that in a closed ring we always have a delocalization transition?

E. Outline

We highlight the theme of negative mobility (NDM/ANM) for *minimal* quasi-one-dimensional networks, with emphasis on the distinction between on-chain and off-chain disorder. The preliminary sections are mainly pedagogical and clarify the dependence of the steady-state current on the bias. This prepares the grounds to the main sections, that expand on the relaxation spectrum and the delocalization transition. The detailed outline is as follows: (1) In Sec. II we elaborate on the NDM/ANM configurations of Figs. 1(b) and 1(c). The model parameters are defined in Eqs. (2)–(9). (2) In Secs. III and IV we derive expressions for the dependence of the current on the bias for a nondisordered chain, and illustrate the NDM/ANM effect. (3) In Sec. IV we consider the effect of disorder on current-vs-bias for the network of Fig. 1(b). This section highlights the possibility to observe an antisliding transition, namely, suppression of the current for bias that exceeds a threshold. (4) In Sec. V we find analytically the relaxation spectrum for a chain that is closed into a nondisordered ring configuration. From that we can re-derive the analytical result for the current, and additionally we get an analytical result for the diffusion coefficient. (5) In Sec. VI we consider the effect of disorder. We explore the possibility to observe an over-damped relaxation and a delocalization transition. We distinguish between on-chain and off-chain disorder. (6) In Sec. VII we further analyze analytically the localization of the relaxation modes, via a reduction to the Anderson-Debye model. The Appendices provide extra technical details. The main results are summarized in Sec. VIII.

II. THE MODEL

The dynamics of the stochastic particle is described by a rate equation,

$$\frac{d}{dt}\mathbf{p} = \mathcal{W}\mathbf{p}, \quad (1)$$

where \mathbf{p} is a vector of probabilities and \mathcal{W} is a matrix of transition rates. The off-diagonal element $w_{n,m}$ of the matrix is the transition-rate from node m to node n . The diagonal

elements $-\gamma_n$ are determined such that the sum over each column is zero. Accordingly γ_n is the total decay-rate from node n .

We consider a *quasi*-one-dimensional chains, as in Fig. 1. Therefore, we have to label the nodes of the network by a composite index. Namely, the nodes are labeled by a site index $n = \text{integer}$ and by an additional index $s = \uparrow, \downarrow$. For a nondisordered chain, by *convention*, all the forward rates to the right are w_o along the chain, and all the outward rates to the dangling sites are c_o . We assume bias f , and *define* the backwards transition rates as $w_o e^{-f}$ and $c_o e^{-\alpha f}$, respectively, where $\alpha > 0$ is a proportionality constant that quantifies the relative sensitivity of the dangling bonds to the bias. We emphasize that without loss of generality the forward rates, by this *convention*, are not affected by the bias. This helps to maintain a numerically meaningful $f \rightarrow \infty$ limit.

Figure 1(b) describes a one-dimensional lattice with dangling bonds. The nonzero transition rates are

$$w_{n\uparrow, n-1\uparrow} = w_n^+ := w_o, \quad (2)$$

$$w_{n-1\uparrow, n\uparrow} = w_n^- := w_o e^{-f}, \quad (3)$$

$$w_{n\downarrow, n\uparrow} = c_n^+ := c_o, \quad (4)$$

$$w_{n\uparrow, n\downarrow} = c_n^- := c_o e^{-\alpha f}. \quad (5)$$

The last expression in each row refers to a nondisordered sample. Note that in our convention bond n connects node n to node $n-1$. The s index can represent a transverse space coordinate, or the possibility of the particle to switch into a nonconducting state.

Figure 1(c) describes a Janus (active) particle that can have forward or backward orientation: in the \uparrow orientation it executes a stochastic self-propelled motion that is biased to the right, while in the \downarrow orientation it executes a stochastic self-propelled motion that is biased to the left. Due to self-propulsion there is some ratio $\exp(\phi) > 1$ between the forward and the backward motion. By our *convention* only the backward rates (relative to the propulsion) are affected, hence the transition rates to the left in the upper edges become $w_o e^{-\phi-f}$, and the transition rates to the right in the lower edges become $w_o e^{-\phi}$. Summarizing, for a nondisordered motion of a Janus particle

$$w_{n\uparrow, n-1\uparrow} = w_{\uparrow}^+ = w_o, \quad (6)$$

$$w_{n-1\uparrow, n\uparrow} = w_{\uparrow}^- = w_o e^{-f-\phi}, \quad (7)$$

$$w_{n\downarrow, n-1\downarrow} = w_{\downarrow}^+ = w_o e^{-\phi}, \quad (8)$$

$$w_{n-1\downarrow, n\downarrow} = w_{\downarrow}^- = w_o e^{-f}, \quad (9)$$

while the c^\pm are given by Eqs. (4) and (5).

Different types of disorder can be introduced as discussed thoroughly for a simple chain [29], and for the configuration of Fig. 1(c) [24]. In the present work, referring to Fig. 1(b), the interesting distinction is between on-chain disorder and off-chain disorder. On-chain disorder means that the bias field f has uncorrelated values f_n on the different bonds of the chain, as in the standard Sinai model. Specifically we assume box

distribution with average value f that reflects the presence of an externally applied bias, plus a random component due to the embedding environment. Accordingly, we write

$$f_n = f + \text{random}[-\sigma, \sigma]. \quad (10)$$

Off-chain disorder is similarly defined. Optionally we can regard it as arising from random α . Namely, in the presence of an external bias f , the stochastic field on the n th dangling bond is $\alpha_n f$ with random values for α_n . Otherwise, we can specify separately σ_{on} for the random field on the chain bonds, and σ_{off} for the random field on the dangling bonds. Which convention is used is a matter of context, per the assumed physical setup.

III. THE STEADY-STATE CURRENT FOR A NONDISORDERED CHAIN

The nonequilibrium steady state (NESS) is determined by the equation $\mathcal{W}\mathbf{p} = 0$, which is formally a continuity equation. For the prototype percolating network of Fig. 1(b), the drift velocity along the chain sites is

$$v_{\uparrow} = (1 - e^{-f})w_o. \quad (11)$$

Without dangling bonds the occupation probability at each site of the chain is $p_{\text{chain}} = 1/L$, where L is the length of the chain, hence the current is $I = (1/L)v_{\uparrow}$. With added dangling bonds the NESS equation implies $p_{\downarrow}/p_{\uparrow} = e^{\alpha f}$, hence

$$p_{\uparrow} = \frac{1}{L} \left(\frac{1}{1 + e^{\alpha f}} \right), \quad (12)$$

and accordingly

$$I = p_{\uparrow} v_{\uparrow} = \frac{w_o}{L} \left(\frac{1 - e^{-f}}{1 + e^{\alpha f}} \right). \quad (13)$$

For the network of Fig. 1(c) the same NESS occupation prevails, but the current becomes

$$I = p_{\uparrow} v_{\uparrow} - p_{\downarrow} v_{\downarrow} \quad (14)$$

$$= \frac{w_o}{L} \left(\frac{[1 - e^{-\phi-f}] + e^{\alpha f} [e^{-\phi} - e^{-f}]}{1 + e^{\alpha f}} \right). \quad (15)$$

For small f we get a linear relation $I \approx Gf$, with

$$G = \frac{w_o}{2L} [(1+\alpha)e^{-\phi} + (1-\alpha)]. \quad (16)$$

We conclude that ANM will show up if $\alpha > 1$ provided the propulsion is strong enough, namely,

$$\phi > \ln \left(\frac{\alpha+1}{\alpha-1} \right). \quad (17)$$

Several I versus f plots are displayed in Fig. 2(a). For completeness we also plot the diffusion coefficient \mathcal{D} in Fig. 2(b). The way to calculate \mathcal{D} will be explained in Sec. V.

IV. THE STEADY-STATE CURRENT FOR A DISORDERED CHAIN

We consider again the network of Fig. 1(b) but now with Sinai disorder. This means on-chain disorder that is given by Eq. (10) and an additional off-chain disorder (due to random

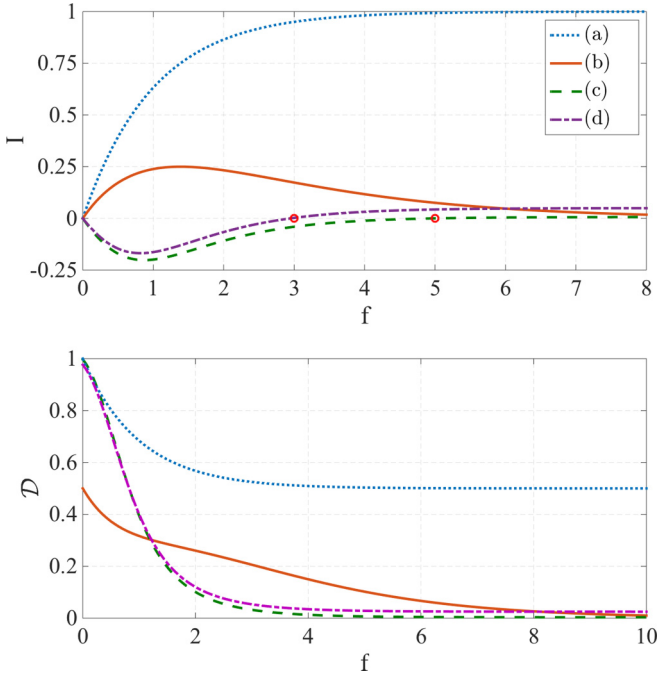


FIG. 2. Current and diffusion versus bias. The *upper* panel displays the current in units of w_o/L , plotted versus the bias f . The curves are for: (a) simple chain with no dangling bonds; (b) chain with dangling bonds ($\alpha = 1/2$); (c) active chain with $\alpha = 2$ and $\phi = 5$; (d) active chain with $\alpha = 2$ and $\phi = 3$. For the active chain $c_o = w_o$, and the red circles indicate the current reversal. The *lower* panel displays, respectively, the diffusion coefficient \mathcal{D} in units of w_o .

α) that will be specified later on. Our objective is to determine the steady-state current I in the presence of disorder and to see whether it diminishes if the bias is below or above some thresholds. Recall that the NESS is determined by the equation $\mathcal{W}\mathbf{p} = 0$, which is formally a continuity equation. Along the n th dangling bond it is implied that

$$\frac{p_{n,\downarrow}}{p_{n,\uparrow}} = e^{\alpha_n f}, \quad (18)$$

because the NESS current there has to be zero. Along the n th bond of the chain we require

$$w_n^+ p_{n-1,\uparrow} - w_n^- p_{n,\uparrow} = I. \quad (19)$$

If one drops the \downarrow dangling sites, then this equation with the normalization $\sum_n p_n = 1$ leads to a solution p_n , that is formally identical to the solution that has been obtained by Derrida [31] for a simple ring. Namely, the current is $I = (1/L)v$, where

$$v = \left(1 - \left\langle \frac{w_n^-}{w_n^+} \right\rangle\right) \left\langle \frac{1}{w_n^+} \right\rangle^{-1} \quad (20)$$

$$= \left(1 - \frac{1}{L} \sum_n e^{-f_n}\right) w_o. \quad (21)$$

This expression is valid if it gives a nonnegative result. It should be realized that $\langle e^{-f_n} \rangle$ is larger than unity if the f_n have zero or small enough average. Consequently, for small bias the above expression becomes negative, indicating that $v = 0$ in

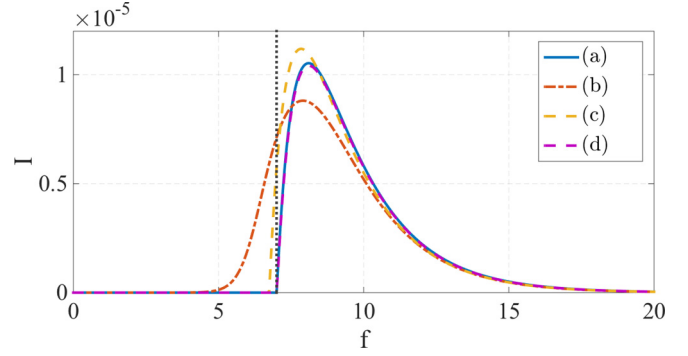


FIG. 3. Sliding transition for a chain with dangling bonds. The current in units of w_o/L is plotted versus the bias f with $\sigma = 10$ and $\alpha = 1/2$. (a) Analytical curve plotted by Eq. (26). (b) Numerical results with a realization of $L = 35$. (c) Analytical results evaluated by Eq. (25) with the same realization as panel (b). (d) Analytical results evaluated by Eq. (25) with $L = 25,000$. The dotted line is $f_s \approx 7$.

the $L \rightarrow \infty$ limit. The transition from zero drift velocity to finite drift velocity as the bias exceeds a threshold is known as the *sliding transition* [31–33].

If we place back the dangling sites, then the solution of Eq. (19) will be the same up to a factor, namely,

$$p_{n,\uparrow} = P_{\uparrow} p_n, \quad (22)$$

where p_{\uparrow} is determined by the normalization condition

$$\sum_{n,s} p_{n,s} = \sum_n (1 + e^{\alpha_n f}) p_{n,\uparrow} = 1. \quad (23)$$

The off-chain disorder α_n is assumed to be independent of the on-chain disorder. We therefore can factorize the ensemble average and deduce that

$$p_{\uparrow} = \frac{1}{L} \left(\frac{1}{1 + \langle e^{\alpha_n f} \rangle} \right). \quad (24)$$

Consequently, for the current we get

$$I = p_{\uparrow} v = \frac{w_o}{L} \left(\frac{1 - \langle e^{-f_n} \rangle}{1 + \langle e^{\alpha_n f} \rangle} \right). \quad (25)$$

This expression still features the Derrida sliding transition, but it can also provide an antisliding transition for large bias, if $\langle e^{\alpha_n f} \rangle$ becomes infinite. As in the case of the standard Sinai model [30–33], also here both the sliding and the antisliding transitions become sharp only in the limit of a large chain ($L \rightarrow \infty$).

Both the sliding transition and the antisliding transition are demonstrated in Figs. 3 and 4. In Fig. 3 we assume that the f_n are box distributed within $[f - \sigma, f + \sigma]$, and that the $\alpha_n f$ are similarly distributed within $[\alpha f - \sigma, \alpha f + \sigma]$, we get

$$I = \frac{w_o}{L} \left(\frac{1 - [\sinh(\sigma)/\sigma] e^{-f}}{1 + [\sinh(\sigma)/\sigma] e^{\alpha f}} \right). \quad (26)$$

Here we have only a sliding transition because the denominator does not diverge for finite bias. In Fig. 4 we assume a stretched distribution for the dangling bonds, namely, we

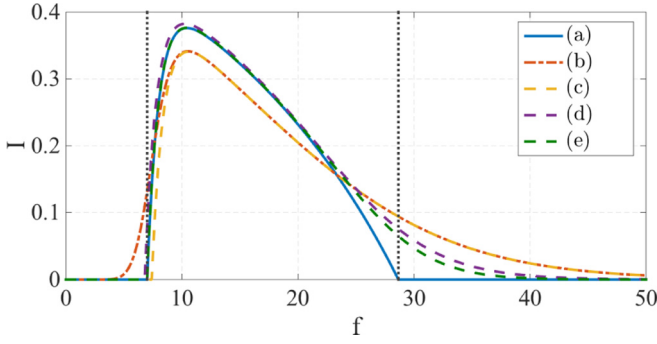


FIG. 4. Antisliding transitions for a chain with stretched distribution of dangling bonds. The current in units of w_o/L is plotted versus the bias f with $\sigma = 10$ and $\alpha = 0.035$. (a) Analytical curve plotted by Eq. (29). (b) Numerical results with a realization of $L = 35$. (c) Analytical results evaluated by Eq. (25) with the same realization as panel (b). (d) Analytical results evaluated by Eq. (25) with $L = 500$. (e) Analytical results evaluated by Eq. (25) with $L = 25\,000$. The dotted lines are $f_s \approx 7$ (left) and $f_c \approx 28.65$ (right).

assume that the $\alpha_n f$ have exponential distribution with an average αf . Accordingly,

$$\langle e^{\alpha_n f} \rangle = \frac{1}{\alpha f} \int_0^\infty e^{f'} e^{-f'/(\alpha f)} df' \quad (27)$$

$$= \begin{cases} \frac{1}{1-\alpha f} & \alpha f < 1 \\ \infty & \alpha f > 1 \end{cases} \quad (28)$$

Here the expectation values diverges for large f , and therefore for larger f the current vanishes. At the regime where the current is finite we get

$$I = \frac{w_o}{L} \left[\frac{1-\alpha f}{2-\alpha f} \right] (1 - [\sinh(\sigma)/\sigma] e^{-f}). \quad (29)$$

This expression gives nonzero result within the range $f_s < f < f_c$, where

$$f_s = \ln[\sinh(\sigma)/\sigma], \quad (30)$$

$$f_c = [1/\alpha]. \quad (31)$$

Again, we emphasize that those sharp transitions appear only in the limit $L \rightarrow \infty$.

V. RELAXATION SPECTRUM FOR A NONDISORDERED RING

Up to now we have focused on the NESS, which is the $\lambda = 0$ eigenstate of \mathcal{W} . Now we turn to discuss the whole spectrum. From the full spectrum we can derive results not only for the drift velocity, but also for the diffusion coefficient. Furthermore, it is the spectrum that contains the information on the delocalization transition, and in particular on whether the relaxation is over-damped or under-damped. We first address the nondisordered version of Fig. 1(b).

The relaxation modes are the right eigenvectors of \mathcal{W} , and they satisfy the equation $\mathcal{W}\Psi = -\lambda\Psi$. In the absence of disorder, due to Bloch theorem, the matrix becomes block diagonal (see Appendix A). Consequently, the eigenvalues are labeled as $\lambda_\nu(k)$, where k is the wave number (the Bloch

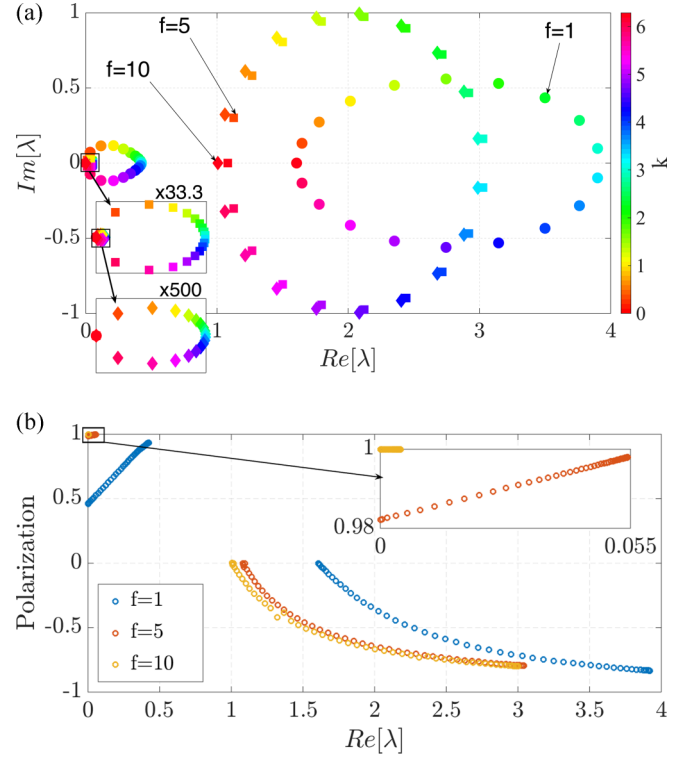


FIG. 5. The relaxation spectrum for a nondisordered ring with dangling bonds. In panel (a) we display in the complex plane the eigenvalues $\lambda_\nu(k)$ for a system of length $L = 100$. Here and in the next figures $w_o = c_o = 1$ and $\alpha = 1/2$. There are three spectra that correspond to $f = 1$ (circles), $f = 5$ (squares), and $f = 10$ (diamonds). The points are color-coded by k . Panel (b) displays the polarization of the associated eigenmodes.

phase), and $\nu = 0, 1$ is the band index. For each k we have to diagonalize a 2×2 matrix:

$$\mathcal{W}^{(k)} = \begin{pmatrix} (e^{-ik}-1)w^+ + (e^{ik}-1)w^- - c^+ & c^- \\ c^+ & -c^- \end{pmatrix}. \quad (32)$$

The result of the diagonalization is demonstrated graphically in Fig. 5. The NESS is the eigenstate that is associated with $\lambda_{0,0} = 0$. The two bands of the spectrum form two complex bubbles in the complex λ plane. The points are color-coded by the Bloch phase k . The second panel in Fig. 5 provides further information on the polarization of the eigenmodes, which is defined as $D = |\Psi_\downarrow|^2 - |\Psi_\uparrow|^2$, where the eigen-vector $\Psi \mapsto (\Psi_\uparrow, \Psi_\downarrow)$ of $\mathcal{W}^{(k)}$ assumes standard normalization. Note that the two bands have opposite polarity. In particular note that the NESS is polarized “positively,” reflecting that the bias expels the probability from the chain and push it into the dangling sites.

The boundaries of the two bands are displayed in Fig. 6, and are based on the expressions that can be found in Appendix B. Our interest is mainly in the $\nu = 0$ band that is bounded from below by $\lambda = 0$. Its complexity implies under-damped relaxation in the long time limit. For large bias it becomes tiny, implying a longer relaxation time.

The weighted drift velocity can be calculated from the spectrum [38]. The result is in agreement with Eq. (13), indicating that the math is self-consistent: Different ways lead

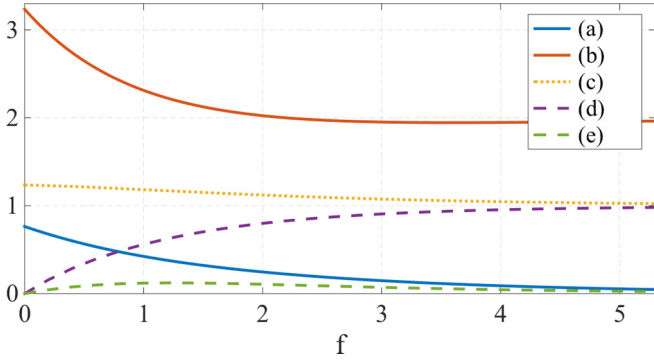


FIG. 6. The band boundaries of the spectrum versus bias. The boundaries of the two bands that are displayed in Fig. 5 are plotted versus f : (a) $\lambda_0(\pi)$; (b) $\lambda_1(\pi) - \lambda_1(0)$; (c) $\lambda_1(0) - \lambda_0(\pi)$; (d) $\max[\text{Im}(\lambda_{\nu=1})]$; (e) $\max[\text{Im}(\lambda_{\nu=0})]$. The $\nu = 0$ band is responsible for the long-time under-damped relaxation. It becomes tiny for large bias, implying a longer relaxation time.

to the same expression. Namely,

$$v = i \left. \frac{\partial \lambda_0(k)}{\partial k} \right|_{k=0} = w_o \left(\frac{1 - e^{-f}}{1 + e^{\alpha f}} \right). \quad (33)$$

The diffusion coefficient can be calculated as well:

$$\begin{aligned} \mathcal{D} &= \left. \frac{1}{2} \frac{\partial^2 \lambda_0(k)}{\partial k^2} \right|_{k=0} \\ &= \left[\frac{1 + e^{-f}}{1 + e^{\alpha f}} \right] \frac{w_o}{2} + \left[\frac{(1 - e^{-f})^2}{(1 + e^{\alpha f})^3} e^{2\alpha f} \right] \frac{w_o^2}{c_o}. \end{aligned} \quad (34)$$

Figure 2 illustrates the f dependence of the above expressions that were derived for the network of Fig. 1(b), and also the result (see Appendix B) that applies to the network of Fig. 1(c). In a simulation we can visualize the evolving probability distribution as a stretching cloud. The second term in Eq. (34), that diverges in the $c_o \rightarrow 0$ limit, reflects the departure of a drifting piece along the chain, from remnants that lags in the dangling bonds. The first term reflects the extra spreading of the drifting piece. In the zero bias limit ($f \rightarrow 0$) it is only the latter contribution that survives, leading to $\mathcal{D} \rightarrow 1/2$.

VI. RELAXATION SPECTRUM FOR A DISORDERED RING

In the absence of disorder the spectrum of a biased system features a “complex bubble” that touches the origin, indicating finite drift velocity and under-damped relaxation. Adding disorder some of the eigenmodes become localized, and the associated eigenvalues become real. If the “complex bubble” is diminished near the origin, then over-damped relaxation is implied.

In the model of Fig. 1(b) the forward and backward transition rates w_n^\pm are along the n th bond that connects the n and $n - 1$ sites, while the c_n^\pm are for the forward and backward rates along the dangling bonds. Namely,

$$w_n^+ = w_o, \quad (35)$$

$$w_n^- = w_o e^{-f_n}, \quad (36)$$

$$c_n^+ = c_o, \quad (37)$$

$$c_n^- = c_o e^{-g_n}. \quad (38)$$

We assume that the f_n contain random box-distributed on-chain disorder due to environmental irregularities, as defined in Eq. (10), while the $g_n = \alpha f + \text{random}[-\sigma, \sigma]$ reflect off-chain disorder with the same distribution. We use $\alpha = 1/2$ in the subsequent numerics. Representative results for the spectrum are presented in Fig. 7. Each point is color-coded by the participation number (PN), namely, the number of units cells that are occupied by the associated eigenmode. With standard normalization the definition is

$$\text{PN} = \left(\sum_n Q_n^2 \right)^{-1}, \quad Q_n = |\psi_{n\uparrow}|^2 + |\psi_{n\downarrow}|^2. \quad (39)$$

We see clearly that large PN is correlated with complexity. This is expected from the general phenomenology of the delocalization transition [36], namely, a localized eigenstate is effectively living on a disconnected ring, for which the asymmetry of the transition can be gauged-away (the technical aspect will become clear in the next section, where we discuss the secular equation for the eigenvalues). We note that the average polarization of the eigenmodes (numerical results not displayed) is similar to that of a nondisordered case [see Fig. 5(b)].

Figure 8 displays the fraction of complex eigenvalues. The fraction is calculated separately for each band. If the bands are not separated by a gap, then we use median for their practical definition. Namely, 50% of the eigenvalues that have the lowest $\text{Re}[\lambda]$ are defined as the $\nu = 0$ band, bounded from above by a vertical dotted line in Fig. 7(a). For on-chain disorder the delocalization transition is clearly resolved if the disorder is strong enough. Namely, up to some critical value of f the complex bubble that touches the origin disappears, and the eigenvalues there become real. Complex eigenvalues with large $\text{Re}[\lambda]$ may exist: They represent a transient under-damped relaxation. For long times the predominant dynamical behavior is over-damped if the bias is below the delocalization threshold. We see that such delocalization transition does not appear if we have only off-chain disorder. In the latter case a small complex bubble that touches the origin survives even if the disorder is large, irrespective of the bias. For strong bias the $\nu = 0$ band exhibits complexity saturation, meaning that a finite fraction of real eigenvalues survives. This complexity saturation will be explained by reduction to the standard case (see next section). In contrast the $\nu = 1$ band becomes 100% complex irrespective of the disorder type.

VII. THE LOCALIZATION OF THE EIGENMODES

To analyze the delocalization that we observe in Fig. 8 for the model of Fig. 1(b), we show that its characteristic equation, $\det(\lambda + \mathcal{W}) = 0$, can be reduced to that of an effective Sinai model [Fig. 1(a)]. Then we can follow the same strategy as in Refs. [29,34–36] that relates the (possibly complex) spectrum of the non-Hermitian matrix \mathcal{W} to the real spectrum of an associated Hermitian matrix \mathbf{H} . We note that a localized eigenmode is effectively living on a disconnected ring. For a disconnected ring the spectrum of \mathcal{W} is identical to the spectrum of $-\mathbf{H}$ and therefore has to be real. This is

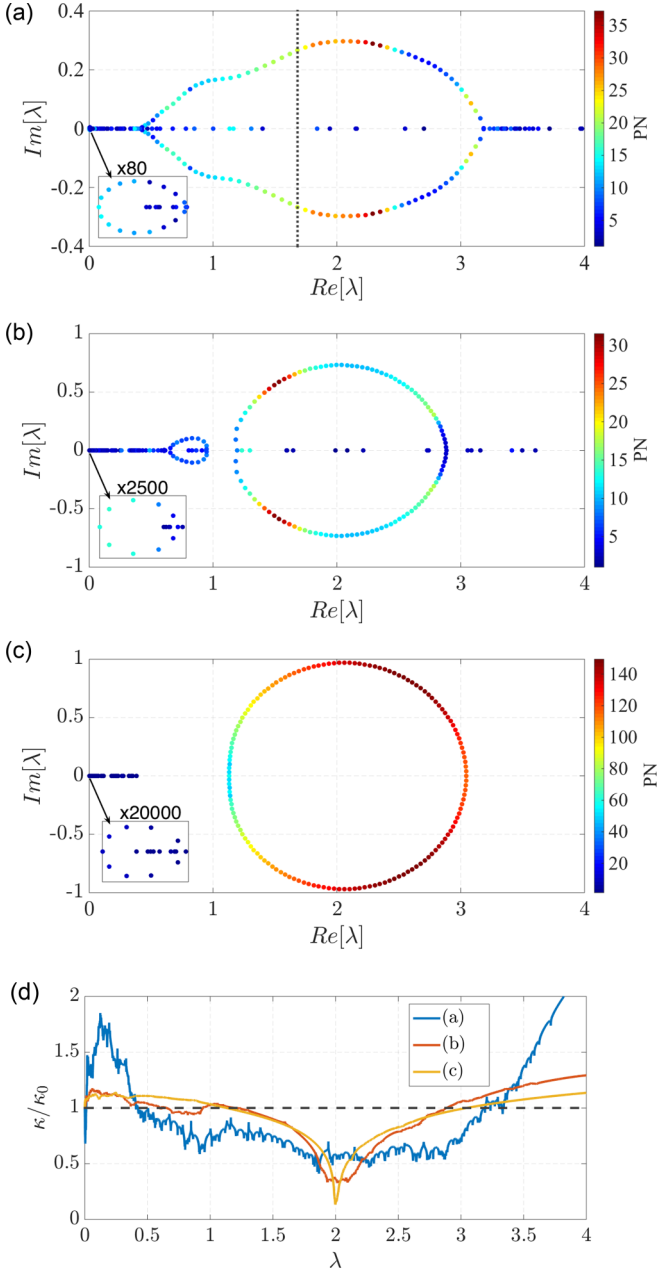


FIG. 7. The relaxation spectrum for a disordered ring with dangling bonds. We display in the complex plane the eigenvalues for a system of length $L = 150$. The other parameters are the same as for the ring of Fig. 5, with added off-chain disorder of strength $\sigma = 5$. Panels (a), (b), and (c) are for $f = 1, 5, 10$, respectively. The points are color-coded by the participation number (PN), namely, the number of units cells that are occupied by the eigenmodes. The vertical dotted line in panel (a) is a median that divides the spectrum into two equal groups. The spectrum separates into two bands in panels (b, c). Panel (d) is related to the analysis in Sec. VII. The inverse localization length is defined by Eq. (48), and calculated from the \mathcal{W} of panels (a), (b), and (c). Complex roots are expected if $\kappa(\lambda) < \kappa(0)$.

the reason for associating the term “delocalization” with the complexity of the spectrum.

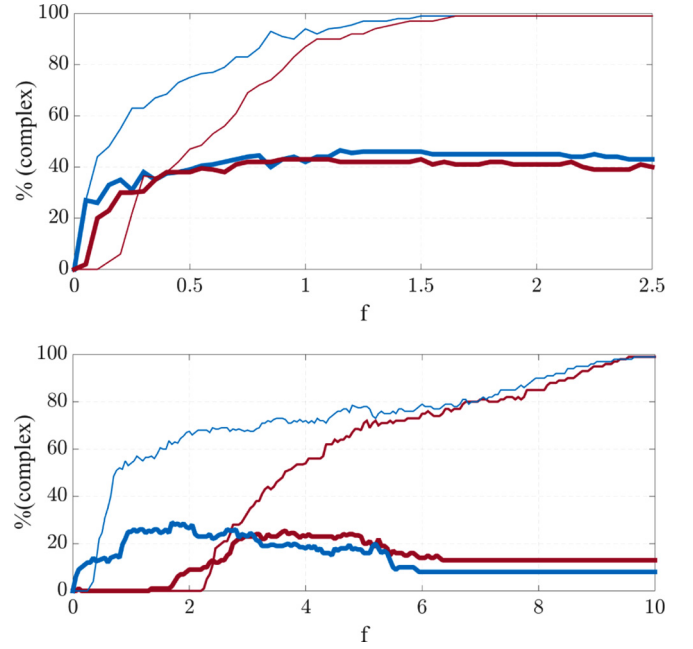


FIG. 8. Delocalization of the eigenstates. The fraction of complex eigenvalues (indicating delocalized eigenstates) is calculated separately for each band (thicker lines for $\nu = 0$). If the bands are not separated, then we use median for their practical definition. The upper and lower panels are for disorder of strength $\sigma = 1, 5$, respectively. Both off-chain (blue) and on-chain (red) disorder are considered. For on-chain disorder the delocalization transition is clearly resolved for $\sigma = 5$, while for off-chain disorder the $\nu = 0$ band always feature a complex bubble. For strong bias the $\nu = 0$ band exhibits complexity saturation, while the $\nu = 1$ band becomes 100% complex irrespective of the disorder type.

A. The Reduction

The equation $\mathcal{W}\psi = -\lambda\psi$ for the eigenmodes of a chain with dangling bonds is

$$\begin{aligned} w_n^+ \psi_{n-1} + w_{n+1}^- \psi_{n+1} + c_n^- \psi_{n,\downarrow} - \gamma_n \psi_n &= -\lambda \psi_n, \\ c_n^+ \psi_n - c_n^- \psi_{n,\downarrow} &= -\lambda \psi_{n,\downarrow}, \end{aligned}$$

where $\gamma_n = w_{n+1}^+ + w_n^- + c_n^+$, and we have used the simplified notation $\psi_n \equiv \psi_{n,\uparrow}$. Eliminating the dangling bonds from the set of coupled equations we get the single-channel tight binding equation

$$w_n^+ \psi_{n-1} + w_{n+1}^- \psi_{n+1} - u_n(\lambda) \psi_n = -\lambda \psi_n, \quad (40)$$

with

$$\begin{aligned} u_n(\lambda) &\equiv [w_{n+1}^+ + w_n^- + c_n^+] - \frac{c_n^+ c_n^-}{c_n^- - \lambda} \\ &\approx (1 + e^{-f_n}) w_o - \lambda e^{g_n}. \end{aligned} \quad (41)$$

The second line above is a small λ expansion. We see that off-chain disorder (random g_n) introduces diagonal disorder of intensity that is proportional to λ^2 , while on-chain disorder (random f_n) does not vanish in this limit. This already explains qualitatively why the λ spectrum is hardly affected by off-chain disorder in the vicinity of the origin.

B. The Spectral determinant

We proceed with a quantitative treatment of the characteristic equation $\det(\lambda + \mathcal{W}) = 0$. After the reduction to a single-channel tight binding model it takes the form $\det(\lambda + \mathbf{W}) = 0$. The $N \times N$ matrix \mathbf{W} (note the different font), with $N = L$, is associated with the reduced equation, namely, Eq. (40). For the calculation of the determinant it is convenient to write the forward and backward rates as $w_n \exp(\pm f_n/2)$, where

$$w_n \equiv \sqrt{w_n^+ w_n^-} = w_o \exp(-f_n/2). \quad (43)$$

The affinity is defined as $\sum_n f_n = Nf$, where f is what we called ‘‘bias.’’ Then it is possible to define an associated Hermitian matrix $-\mathbf{H}$ that has the same diagonal elements, while the off-diagonal couplings are w_n . A linear-algebra formula [39] (optionally see Appendix C of Ref. [37]) leads to the identity

$$\det(\lambda + \mathbf{W}) = \det(\lambda - \mathbf{H}) - [e^{Nf/2} + e^{-Nf/2} - 2] \prod_n (-w_n). \quad (44)$$

C. Finding the eigenvalues

It is convenient to define the average coupling as

$$w_{\text{avg}} = \left[\prod_{n=0}^N w_n \right]^{1/N}. \quad (45)$$

Then the characteristic equation takes the form

$$\prod_{k=0}^N \left(\frac{\lambda - \epsilon_k(\lambda; f)}{-w_{\text{avg}}} \right) = 2 \left[\cosh \left(\frac{Nf}{2} \right) - 1 \right], \quad (46)$$

where ϵ_k are the real eigenvalues of the Hermitian \mathbf{H} matrix. A numerical demonstration of this (*exact*) equation is provided in Fig. 9. Its left-hand side, up to factor, is the spectral determinant $Z(\lambda) = \det(\lambda - \mathbf{H})$. The right-hand side is a constant Z_0 that is represented by a dashed horizontal line. Note that the dashed line intersects the spectral determinant at $\lambda = 0$, which corresponds to the NESS, hence $Z_0 = Z(0)$. The nontrivial *real* eigenvalues of \mathcal{W} are determined by the intersection of $Z(\lambda)$ with the dashed line.

In the absence of dangling bonds $Z(\lambda)$ is a polynomial with roots ϵ_k that do not depend on λ . In such case it oscillates around zero with some *envelope*. Taking the log of this envelope we define a function $\kappa(\lambda)$ such that

$$|Z(\lambda)| \lesssim w_{\text{avg}}^N e^{N\kappa(\lambda)}. \quad (47)$$

In Fig. 9(b), up to $\lambda \sim 2.6$ the envelope of $Z(\lambda)$ is well below the dashed line, and consequently all the eigenvalues in this region are complex. More generally there might be regions where the envelope is above the dashed line, and then we get real eigenvalues, as demonstrated in Fig. 7.

Due to the elimination of the dangling bonds the ϵ_k acquire λ dependence: For each λ we have to calculate again the $\epsilon_k(\lambda; f)$ spectrum. The most conspicuous implication is the appearance of singular spikes at $\lambda = c_n^-$. For large enough f those spikes invade the lower band of the spectrum, as demonstrated in Fig. 9(b). Extra real eigenvalues that coexist

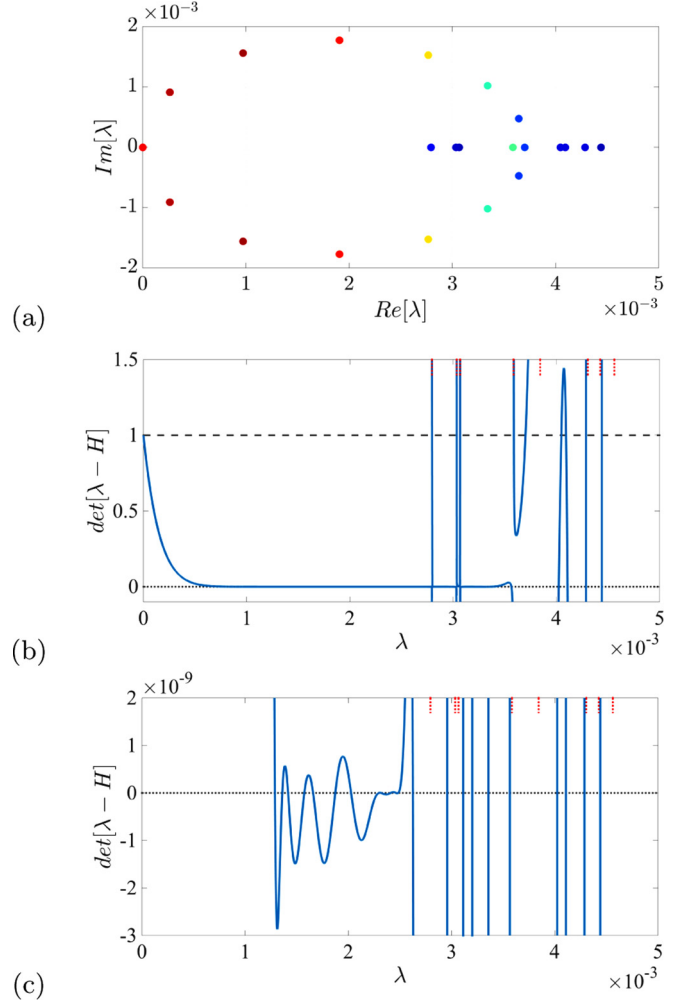


FIG. 9. Spectral determinant for off-chain disorder. We consider an $L = 150$ system with off-chain disorder $\sigma = 5$ and $f = 2$. Panel (a) displays a the relaxation spectrum, focusing in the $\lambda \sim 0$ region where complex and real eigenvalues coexist. Panel (b) displays the spectral determinant $\det(\lambda - \mathbf{H})$ along the real axis. Each intersection with the dashed line implies a real eigenvalue of \mathcal{W} (see text for further details). The upper bars indicate the values $\lambda = c_n^-$ at which the determinant diverges. Panel (c) provides a vertical zoom.

with the complex bubble are implied. Those real eigenvalues corresponds to over-damped relaxation modes that are localized on the dangling sites.

D. The Thouless relation

Following Ref. [36] we point out that the log of the left-hand side in Eq. (46), after dividing by N , is the Thouless formula [40,41] for the inverse localization length κ in the Hermitian problem. Substitution of the definition of w_n leads to

$$\kappa(\lambda) = \frac{f}{2} + \frac{1}{N} \sum_{k=0}^N \ln \left| \frac{\lambda - \epsilon_k(\lambda; f)}{w_o} \right|. \quad (48)$$

A few words are in order regarding the use of this formula. It is implicit that we refer here to the *envelope* of the spectral determinant. Furthermore, the identification of $\kappa(\lambda)$ as the

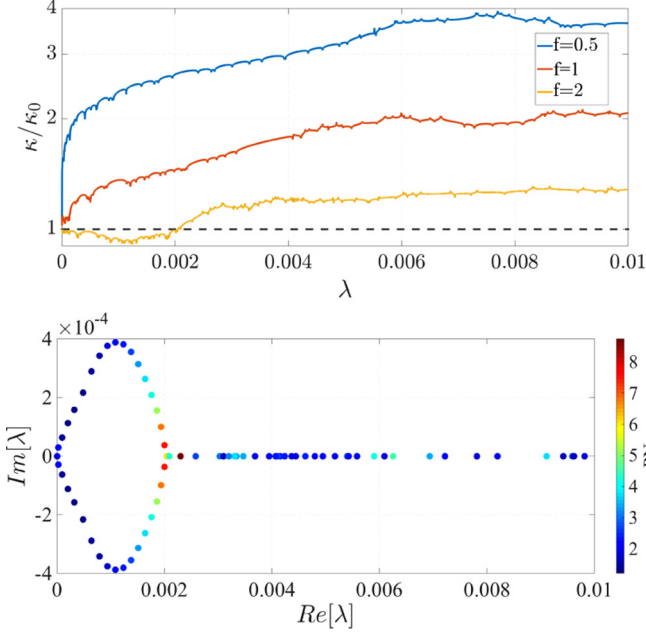


FIG. 10. The inverse localization length for on-chain disorder. We consider an $L = 300$ chain with both off-chain and on-chain disorder $\sigma = 5$. The inverse localization length $\kappa(\lambda)$ of Eq. (48) is calculated in the λ range of the $\nu = 0$ band. The bias $f = 0.5, 1, 2$ is indicated in the legend. In the lower panel we display the spectrum for $f = 2$. The spectrum is complex in the range where $\kappa(\lambda) < \kappa(0)$.

inverse localization length is meaningful only in the λ range where the (real) spectrum stretches, otherwise it is a merely a formal continued expression.

Traditionally κ is determined using a transfer matrix method. There are also some analytical approximations that can be used (see next paragraph). But for our purpose a direct numerical calculation using the Thouless formula is most convenient. The reduction of the \mathcal{W} -problem to the \mathbf{H} -problem assumes real λ , hence Eq. (46) provides real roots if $\kappa(\lambda) > \kappa(0)$; otherwise, complex spectrum should appear (which cannot be extracted directly by inspection). This expectation is confirmed numerically by Figs. 10 and 11, where we contrast the delocalization scenario for on-chain disorder with the scenario that is observed for off-chain disorder. In the latter case there is always a small range near the origin where $\kappa(\lambda) < \kappa(0)$, leading to the appearance of a complex bubble that implies under-damped relaxation.

E. The inverse localization length

As mentioned above, there are some analytical approximations that can be used to evaluate κ . Exact results are available in the continuum limit, which is not useful here. We are therefore satisfied with a standard Born approximation that is based on a Fermi-Golden-Rule picture:

$$\kappa(\lambda) = \frac{\sigma_{\parallel}^2}{8\bar{w}^2 k_{\lambda}^2} + \frac{\sigma_{\perp}^2}{8\bar{w}^2} k_{\lambda}^2. \quad (49)$$

Those are Eqs. (14) and (15) of Ref. [42], where further refinements are discussed, and additional references therein. This equation requires a careful explanation. It is expressed

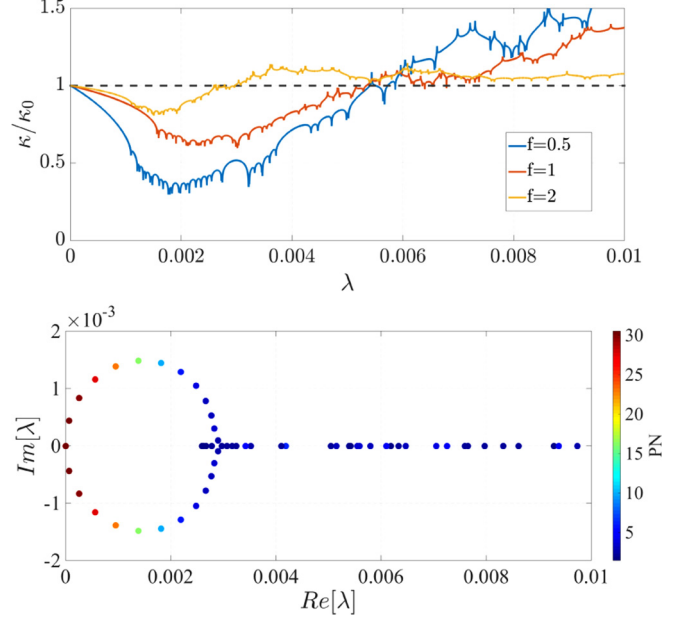


FIG. 11. Inverse localization length for off-chain disorder. The same as for Fig. 10, but with only off-chain disorder. Here the spectrum has a complex fraction for any f .

in terms of the wave number that is determined by the dispersion relation $\lambda = 2\bar{w}[1 - \cos(k)]$, where \bar{w} is the harmonic average over the bond couplings Eq. (43). The approximation $\lambda \approx w_o k^2$ can be used for weak disorder in the small wavelength regime. The two terms in Eq. (49) correspond to on-diagonal and off-diagonal disorder, respectively. We discuss the two terms separately below.

The Hermitian real matrix \mathbf{H} is formally identical to that of the Anderson-Debye model; see Appendix C. The *off-diagonal disorder*, a.k.a., resistor network disorder, is the same type of disorder that appears, e.g., in the Debye model (balls connected by springs). The strength of this disorder is defined as follows:

$$\sigma_{\perp}^2 \equiv \bar{w}^4 \text{Var} \left[\frac{1}{w_n} \right] \approx \frac{1}{4} w_o^2 e^{-f} \text{Var}[f_n]. \quad (50)$$

This definition assumes that the bonds are uncorrelated. The approximation is based on first order treatment of the disorder in Eq. (43). Looking at Eq. (49) we see that its effect is significant for the short-wavelength modes, and can be neglected in the vicinity of $\lambda = 0$. It is the same as in the Debye model where it is argued that the long-wavelength modes tend to be extended.

The *on-diagonal disorder* is more subtle. In the standard Anderson model all bonds are identical and it is common to consider white on-site disorder. Here it is not the case, hence the definition for the strength of the disorder becomes more subtle:

$$\sigma_{\parallel}^2 \equiv \text{Var}_{\lambda} [u_n - w_n - w_{n+1}]. \quad (51)$$

If \mathbf{H} were a stochastic kernel that preserve probability, then we would get from this expression $\sigma_{\parallel} = 0$ and would be left with Debye-type localization only. We have extra diagonal disorder analogous to pinning of the balls to the ground in

the Debye model. This extra disorder leads to Anderson-type localization at the vicinity of $\lambda = 0$. The second issue to notice is the subscript in Var_λ . This subscript reminds us that the diagonal elements are not independent random variables. Consequently, we do not have “white disorder” and the variance has to be calculated at the “energy” of interest. Namely, the Born approximation Eq. (49) is based on evaluation of matrix elements $\langle -k|U(x)|k \rangle$ for backscattering. Here we use for clarity continuous space notations (x instead of n). Averaging the squared matrix elements over realizations of the potential $U(x)$ one deduces that

$$\text{Var}_\lambda[U(x)] = \sum_r e^{ikr} C(r), \quad (52)$$

where $C(r)$ is the correlation function of the disorder. Here we are back with discrete notions, accordingly the distance r between sites is an integer number. For “white” disorder $C(r) = \text{Var}(U_n)\delta_{r,0}$. But the potential U_n in the square brackets of Eq. (51) is correlated. For presentation purpose we assume also $f \ll 1$, which corresponds to the continuum limit, while the more general case is addressed in Appendix D. The disorder in leading order comes out

$$U_n = -\frac{w_o}{2}(f_n - f_{n-1}) - \lambda g_n + \text{const.} \quad (53)$$

Consequently, we obtain

$$\sigma_\parallel^2 \approx \frac{w_o}{4}\lambda \text{Var}[f_n] + \lambda^2 \text{Var}[g_n]. \quad (54)$$

Substitution into Eq. (49) we see, as anticipated, that off-chain disorder provides a contribution proportional to λ that always vanishes in the vicinity of $\lambda = 0$, while on-chain disorder does not vanish.

The bottom line is very simple, and we summarize it in simple words: the inverse localization length is determined by the effective diagonal disorder. The strength of this disorder is proportional to λ^2 for off-chain disorder, and therefore we always get a complex bubble at the vicinity of the origin, indicating under-damped relaxation. For on-chain disorder the inverse localization length approaches a finite value at the limit $\lambda \rightarrow 0$. Therefore, the complexity depends on the slope $\kappa'(0)$ at the origin. This slope becomes negative for large enough f , hence we get a delocalization transition. The details in the latter case are the same as in the “standard model”; see Ref. [29] where also the complexity saturation is explained.

VIII. SUMMARY

Stochastic networks are of general interest in many fields of Physics, as well as in Chemistry and Engineering. Key questions in the study of such networks are how they respond to bias, and what are their relaxation modes. In the traditional studies of tight binding models the main observations have to do with the sliding and the delocalization transitions. Once we allow more complex quasi-one-dimensional configurations, some new issues emerge.

The delocalization of the relaxation modes for the ANM configuration of Fig. 1(c) has been already studied in Ref. [24]. In the present work we have focused on the NDM

configuration of Fig. 1(b), which is the simplest version of a comb-type model [10–13].

In the preliminary pedagogical sections we used the conventional NESS perspective to derive the dependence of the steady-state current on the bias (see, e.g., Figs. 2, 3, and 4). Then we clarified that results for v and D can be regraded as spectral properties that characterize the relaxation spectrum. From this point on our interest has been focused on the study of this spectrum, and specifically in the delocalization transition of the eigenmodes.

The study was partially motivated by the following question: We know that in one dimension we always have localization; does it mean that in a closed ring we always have a delocalization transition? It was essential in this context to distinguish between on-chain disorder and off-chain disorder. In particular, we found that off chain disorder leads to localization that is not strong enough to induce over-damped relaxation, hence delocalization transition is absent. It is implied that for off-chain disorder also sliding transition does not take-place. In fact the absence of sliding transition is much easier for understanding using a NESS-perspective because for off-chain disorder activation barriers are not formed.

On the formal side we have explained how the analysis of the relaxation spectrum can be carried out using a reduced tight binding model. Thus, the relaxation spectrum (eigenvalues of \mathcal{W}) can be related to the real spectrum of a real Hermitian matrix H that describes an effective Anderson-Debye model. To figure out the delocalization transition, the λ dependence of the inverse localization length is required. This dependence is very different for on-chain and off-chain disorder.

ACKNOWLEDGMENT

This research was supported by the Israel Science Foundation (Grant No. 283/18).

APPENDIX A: THE BLOCH MATRIX

For a one-dimensional chain with dangling bonds, in the absence of disorder, the matrix \mathcal{W} can be written using momentum and spin operators. For symmetric transitions,

$$\mathcal{W} = c_o[\sigma_x - 1] + \sum_{\pm} \sigma_{\uparrow} w_o [e^{\pm iP} - 1], \quad (A1)$$

where the momentum operator is defined such that $e^{\mp P}|n\rangle = |n\pm 1\rangle$, and $\sigma_{\uparrow} = \frac{1}{2}[\mathbf{1} + \sigma_z]$ is a projector on the chain sites, while the Pauli operator σ_x induce transitions between \uparrow and \downarrow sites. The momentum with eigenvalue k is a constant of motion, and therefore the matrix decomposed into blocks:

$$\mathcal{W}^{(k)} = \begin{pmatrix} -c^+ + (e^{-ik} - 1)w^+ + (e^{ik} - 1)w^- & c^- \\ c^+ & -c^- \end{pmatrix}. \quad (A2)$$

In the latter expression we have assumed that transitions do not have the same rates in the forward and in the backward directions, and therefore replaced c_o by c^{\pm} , leading to an asymmetric non-Hermitian matrix that describes Fig. 1(b). For the quasi-one-dimensional network of Fig. 1(c) we add the transitions along the \downarrow sites and get

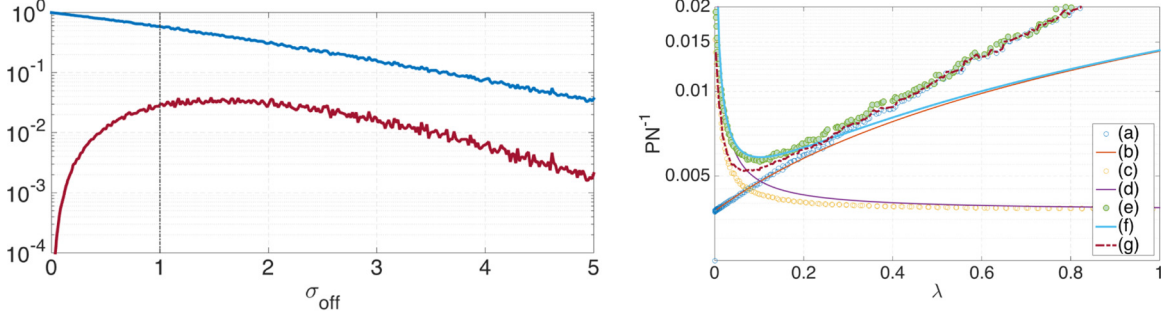


FIG. 12. The perturbative estimate of the PN. Left panel: The dependence of \bar{w} (upper, blue) and σ_{\perp} (lower, red) on σ_{off} . We use harmonic average for the former, and Eq. (50) for the latter. Right panel: The PN is numerically determined for a ring of $L=400$ sites, based on 500 realizations of the disorder. Plots (a) and (c) are for off-diagonal disorder $\sigma_{\text{off}} = 1$ and for on-diagonal disorder $\sigma_{\text{on}} = 0.05$, respectively. Plot (e) is what we get if we have both. Plot (g) corresponds to $\kappa_{\text{off}} + \kappa_{\text{on}}$, based on plots (a) and (c). Curves (b), (d), and (f) are the analytical estimates based on Eq. (49) with no fitting parameters.

$$\mathcal{W}^{(k)} = \begin{pmatrix} -c^+ + (e^{-ik} - 1)w_{\uparrow}^+ + (e^{ik} - 1)w_{\uparrow}^- & c^- \\ c^+ & -c^- + (e^{-ik} - 1)w_{\downarrow}^+ + (e^{ik} - 1)w_{\downarrow}^- \end{pmatrix}. \quad (\text{A3})$$

The diagonalisation of $\mathcal{W}^{(k)}$ provides the $\lambda_v(k)$ spectrum, from which analytical expressions for the drift velocity and the diffusion coefficient are derived.

APPENDIX B: BAND BOUNDARIES

The expressions for the band boundaries, assuming $w_o = c_o = 1$ are

$$\lambda_0(\pi) = \frac{1}{2} e^{-(1+\alpha)f} \left[e^f + 2e^{\alpha f} + 3e^{(1+\alpha)f} + \sqrt{e^{2f} + 4e^{2\alpha f} + 9e^{2(1+\alpha)f} - 2e^{2(2+\alpha)f} - 4e^{(1+\alpha)f} + 12e^{(1+2\alpha)f}} \right], \quad (\text{B1})$$

$$\lambda_1(0) = 1 + e^{-\alpha f}, \quad (\text{B2})$$

$$\lambda_1(\pi) = \frac{1}{2} \left[3 + 2e^{-f} + e^{-\alpha f} - e^{(1+\alpha)f} \sqrt{e^{2f} + 4e^{2\alpha f} + 9e^{2(1+\alpha)f} - 2e^{2(2+\alpha)f} - 4e^{(1+\alpha)f} + 12e^{(1+2\alpha)f}} \right]. \quad (\text{B3})$$

The full expression for $\lambda_0(k)$ is not too illuminating and therefore is not displayed. Its second derivative at $k = 0$ gives the diffusion coefficient \mathcal{D} of Eq. (34) which is plotted in Fig. 2(b). For completeness we write also what is result for the diffusion coefficient for the active network:

$$\mathcal{D} = \left[\frac{(1 + e^{\alpha f - f}) + e^{-\phi}(e^{-f} + e^{\alpha f})}{1 + e^{\alpha f}} \right] \frac{w_o}{2} + \left[\frac{e^{2\alpha f}(1 + e^{-f})^2(1 - e^{-\phi})^2}{(1 + e^{\alpha f})^3} \right] \frac{w_o^2}{c_o}. \quad (\text{B4})$$

APPENDIX C: THE ANDERSON-DEBYE MODEL

What we call Anderson-Debye model refers here to a system whose dynamics is dictated by a real symmetric matrix \mathbf{H} that describes a one-dimensional tight binding chain with both diagonal disorder and off-diagonal disorder, namely,

$$\mathbf{H} = \sum_n |n\rangle u_n \langle n| + \sum_n [|n\rangle w_n \langle n-1| + |n-1\rangle w_n \langle n|]. \quad (\text{C1})$$

The Anderson model arises in the context of electronic conduction: A particle hops with frequency w_n between sites that do not have the same potential u_n . The Debye model refers to balls that are connected by springs that have spring-constants w_n , and that are possibly grounded to the floor with extra springs (a.k.a., pinning). If the disorder is weak, then we define

$$\sigma_{\perp}^2 \equiv \text{Var}[w_n], \quad (\text{C2})$$

$$\sigma_{\parallel}^2 \equiv \text{Var}[u_n - w_n - w_{n+1}]. \quad (\text{C3})$$

In the absence of pinning ($\sigma_{\parallel} = 0$) Debye has correctly conjectured that the low lying excitations ($\lambda \rightarrow 0$) are extended free waves. Otherwise, the eigenstates are localized, as argued by Anderson. Leading order perturbation theory (the Fermi-golden-rule, a.k.a., in this context the Born approximation) leads to Eq. (49) for the inverse localization length.

A slightly improved version of Eq. (49), see Ref. [42], involves the harmonic average \bar{w} for the mean coupling, and Eq. (50) for its dispersion. The rationale of looking on the statistic of $1/w_n$ is based on the formal analogy with a resistor-network (bonds added in series), where rigorously $1/\bar{w}$ is the resistivity of the bond-disordered chain.

The limitations of the perturbative expression Eq. (49) have been pointed out in the main text. For demonstration purpose we test its usefulness in Fig. 12. We consider a chain of length L with

$$w_n = e^{-\text{random}[0, \sigma_{\text{off}}]}, \quad (\text{C4})$$

$$u_n = w_n + w_{n+1} + \text{random}[-\sigma_{\text{on}}, \sigma_{\text{on}}]. \quad (\text{C5})$$

For a nondisordered sample we have $\text{PN}_0 = L$, while for a disordered ring we expect $\text{PN}^{-1} = \text{PN}_0^{-1} + \kappa$; see Ref. [43]. We test both the additivity of κ which is implied by Eq. (49), and also the formula as it is, with no fitting parameters. We conclude that it works reasonably well in the λ range of interest.

APPENDIX D: THE ON-DIAGONAL DISORDER

We write the bias for a chain bonds $f_n = f + \tilde{f}_n$, and for a dangling bonds $g_n = \alpha f + \tilde{g}_n$. Accordingly we have for weak disorder, after dropping a constant,

$$\begin{aligned} U_n &\approx -\frac{w_o}{2} e^{-f/2} [(2e^{-f/2} - 1)\tilde{f}_n - \tilde{f}_{n-1}] - \lambda e^{\alpha f} \tilde{g}_n \\ &\equiv A\tilde{f}_n + B\tilde{f}_{n-1} + C\tilde{g}_n. \end{aligned} \quad (\text{D1})$$

Consequently, we get for the effective strength of the disorder,

$$\sigma_{\parallel}^2 \approx [A^2 + B^2 + 2AB \cos(k)]\text{Var}[f_n] + C^2\text{Var}[g_n]. \quad (\text{D2})$$

In the main text we have highlighted the continuum limit ($f \ll 1$) for which $A \approx -B$, and $\cos(k) \approx 1 - (1/2)k^2$, and therefore the first term is proportional to λ . In general, we might have a term that does not vanish in the limit $\lambda \rightarrow 0$. Then one has to use a formula that goes beyond the diverging approximation of Eq. (49).

-
- [1] L. Esaki, New phenomenon in narrow germanium p-n junctions, *Phys. Rev.* **109**, 603 (1958).
- [2] L. L. Chang, L. Esaki, and R. Tsu, Resonant tunneling in semiconductor double barriers, *Appl. Phys. Lett.* **24**, 593 (1974).
- [3] A. Sibille, J. F. Palmier, H. Wang, and F. Molloy, Observation of Esaki-Tsu Negative Differential Velocity in GaAs/AlAs Superlattices, *Phys. Rev. Lett.* **64**, 52 (1990).
- [4] B. J. Keay, S. Zeuner, S. J. Allen, K. D. Maranowski, A. C. Gossard, U. Bhattacharya, and M. J. W. Rodwell, Dynamic Localization, Absolute Negative Conductance, And Stimulated, Multiphoton Emission in Sequential resonant tunneling semiconductor superlattices, *Phys. Rev. Lett.* **75**, 4102 (1995).
- [5] G. C. Dousmanis, R. C. Duncan, J. J. Thomas, and R. C. Williams, Experimental Evidence for Carriers with Negative Mass, *Phys. Rev. Lett.* **1**, 404 (1958).
- [6] H. Kromer, Proposed negative-mass microwave amplifier, *Phys. Rev.* **109**, 1856 (1958).
- [7] X. L. Lei, N. J. M. Horing, and H. L. Cui, Theory of Negative Differential Conductivity in a Superlattice Miniband, *Phys. Rev. Lett.* **66**, 3277 (1991).
- [8] E. H. Cannon, F. V. Kusmartsev, K. N. Alekseev, and D. K. Campbell, Absolute Negative Conductivity and Spontaneous Current Generation in Semiconductor Superlattices With Hot Electrons, *Phys. Rev. Lett.* **85**, 1302 (2000).
- [9] H. Bottger and V. V. Bryksin, Hopping conductivity in ordered and disordered systems (III), *Phys. Status Solidi (b)* **113**, 9 (1982).
- [10] A. Bunde, S. Havlin, H. E. Stanley, B. Trus, and G. H. Weiss, Diffusion in random structures with a topological bias, *Phys. Rev. B* **34**, 8129 (1986).
- [11] V. Balakrishnan and C. V. D. Broeck, Transport properties on a random comb, *Physica A: Stat. Mech. Appl.* **217**, 1 (1995).
- [12] R. K. P. Zia, E. L. Praestgaard, and O. G. Mouritsen, Getting more from pushing less: Negative specific heat and conductivity in nonequilibrium steady states, *Am. J. Phys.* **70**, 384 (2002).
- [13] G. Ben Arous and A. Fribergh, Biased random walks on random graphs, [arXiv:1406.5076](https://arxiv.org/abs/1406.5076).
- [14] P. Baerts, U. Basu, C. Maes, and S. Safaverdi, Frenetic origin of negative differential response, *Phys. Rev. E* **88**, 052109 (2013).
- [15] A. Sarracino, F. Cecconi, A. Puglisi, and A. Vulpiani, Nonlinear Response of Inertial Tracers in Steady Laminar Flows: Differential and Absolute Negative Mobility, *Phys. Rev. Lett.* **117**, 174501 (2016).
- [16] J. Cividini, D. Mukamel, and H. A. Posch, Driven tracer with absolute negative mobility, *J. Phys. A: Math. Theor.* **51**, 085001 (2018).
- [17] F. Turci, E. Pitard, and M. Sellitto, Driving kinetically constrained models into nonequilibrium steady states, *Phys. Rev. E* **86**, 031112 (2012).
- [18] C. Reichhardt and C. J. O. Reichhardt, Velocity force curves, laning, and jamming for oppositely driven disk systems, *Soft Matter* **14**, 490 (2018).
- [19] S. B. Vrhovac and Z. L. Petrovic, Momentum transfer theory of nonconservative charged particle transport in mixtures of gases, *Phys. Rev. E* **53**, 4012 (1996).
- [20] P. Reimann, R. Kawai, C. V. D. Broeck, and P. Hanggi, Coupled Brownian motors: Anomalous hysteresis and zero-bias negative conductance, *Europhys. Lett.* **45**, 545 (1999).
- [21] R. Eichhorn, P. Reimann, and P. Hanggi, Paradoxical motion of a single Brownian particle: Absolute negative mobility, *Phys. Rev. E* **66**, 066132 (2002).
- [22] P. Hanggi and F. Marchesoni, Artificial Brownian motors: Controlling transport on the nanoscale, *Rev. Mod. Phys.* **81**, 387 (2009).
- [23] B. Cleuren and C. V. D. Broeck, Brownian motion with absolute negative mobility, *Phys. Rev. E* **67**, 055101 (2003).
- [24] D. Shapira, D. Meidan, and D. Cohen, Localization due to topological stochastic disorder in active networks, *Phys. Rev. E* **98**, 012107 (2018).
- [25] A. Walther and H. E. A. Muller, *Janus Particle Synthesis, Self-Assembly, and Applications* (Royal Society of Chemistry, London, 2012), pp. 1–28.
- [26] P. M. Wheat, N. A. Marine, J. L. Moran, and J. D. Posner, Rapid fabrication of bimetallic spherical motors, *Langmuir* **26**, 13052 (2010).
- [27] A. M. Menzel, Tuned, driven, and active soft matter, *Phys. Rep.* **554**, 1 (2015).

- [28] Y. Kafri, D. K. Lubensky, and D. R. Nelson, Dynamics of molecular motors with finite processivity on heterogeneous tracks, *Phys. Rev. E* **71**, 041906 (2005).
- [29] D. Hurowitz and D. Cohen, Percolation, sliding, localization and relaxation in topologically closed circuits, *Sci. Rep.* **6**, 22735 (2016).
- [30] Y. G. Sinai, The limiting behavior of a one-dimensional random walk in a random medium, *Theory Probab. Appl.* **27**, 256 (1983).
- [31] B. Derrida, Velocity and diffusion constant of a periodic one-dimensional hopping model, *J. Stat. Phys.* **31**, 433 (1983).
- [32] J. P. Bouchaud and A. Georges, Anomalous diffusion in disordered media: Statistical mechanisms, models and physical applications, *Phys. Rep.* **195**, 127 (1990).
- [33] J. P. Bouchaud, A. Comtet, A. Georges, and P. L. Doussal, Classical diffusion of a particle in a one-dimensional random force field, *Ann. Phys.* **201**, 285 (1990).
- [34] N. Hatano and D. R. Nelson, Localization Transitions in Non-Hermitian Quantum Mechanics, *Phys. Rev. Lett.* **77**, 570 (1996).
- [35] N. Hatano and D. R. Nelson, Vortex pinning and non-Hermitian quantum mechanics, *Phys. Rev. B* **56**, 8651 (1997).
- [36] N. M. Shnerb and D. R. Nelson, Winding Numbers, Complex Currents, and Non-Hermitian Localization, *Phys. Rev. Lett.* **80**, 5172 (1998).
- [37] D. Hurowitz and D. Cohen, Relaxation rate of a stochastic spreading process in a closed ring, *Phys. Rev. E* **93**, 062143 (2016).
- [38] D. Hurowitz and D. Cohen, Non-equilibrium version of the Einstein relation, *Phys. Rev. E* **90**, 032129 (2014).
- [39] L. G. Molinari, Determinants of block tridiagonal matrices, *Linear Algebra and its Applications* **429**, 2221 (2008).
- [40] D. J. Thouless, A relation between the density of states and range of localization for one dimensional random systems, *J. Phys. C* **5**, 77 (1972).
- [41] C. Texier, Waves in disordered media and localization phenomena, Lecture Notes (2020), <https://www.phys.ens.fr/spip.php?article2344>.
- [42] I. Weinberg, Y. D. Leeuw, T. Kottos, and D. Cohen, Resistor-network anomalies in the heat transport of random harmonic chains, *Phys. Rev. E* **93**, 062138 (2016).
- [43] F. M. Izrailev, T. Kottos, and G. P. Tsironis, Scaling properties of the localization length in one-dimensional paired correlated binary alloys of finite size, *J. Phys.: Condens. Matter* **8**, 2823 (1996).